Modeling Diffusion Between Regions With Different Diffusion Coefficients

Steven S. Andrews

***Abstract*—Biological systems often include spatial regions with different diffusion coefficients. Explicitly simulating their physical causes is computationally intensive, so it is typically preferable to simply vary the coefficients. This raises the question of how to address the boundaries between the regions. Making them fully permeable in both directions seems intuitively reasonable, but causes molecular motion to be simulated as active diffusion, meaning that it arises from energy that is continuously added to the system; in this case, molecules accumulate on the slow-diffusing side. However, molecular motion in most biochemical systems is better described as thermal diffusion, meaning that it occurs even at equilibrium. This can be simulated by reducing the transmission probability into the slow-diffusing side, which yields the correct result that spatially varying diffusion coefficients that arise from macromolecular crowding, changes in viscosity, or other energy-neutral influences do not affect equilibrium molecular concentrations. This work presents transmission coefficients and transmission probability equations for simulating thermal diffusion, including for cases with free energy differences and/or volume exclusion by crowders. They have been implemented in the Smoldyn particle-based simulation software.**

***Index Terms*—Macromolecular crowding, diffusion, biochemical simulation, particle-based simulation, molecular communication.**

I. Introduction

DIFFUSION coefficients in biological systems are not uniform but vary depending on location. For example, diffusion is generally fairly rapid in dilute solution, about 4-fold slower in eukaryotic cells [1], and 15-fold slower in bacterial cells [2]. Compared to the surrounding cytoplasm, diffusion is faster in bacterial nucleoids [3] and slower in phase-separated cytoplasmic droplets [4], [5]. Within membranes, diffusion is slowed by lipid rafts [6] and by nuclear diffusion barriers [7]. On larger size scales, diffusion coefficients vary dramatically across the blood-air barrier in vertebrate lungs and across the blood-brain barrier in vertebrate nervous systems [8]. These varying diffusion coefficients raise the questions: How do they affect chemical concentrations and how can their effects be simulated accurately?

Manuscript received 15 September 2023; revised 9 February 2024; accepted 5 April 2024. Date of publication 15 April 2024; date of current version 25 September 2024. This work was supported in part by the National Institute of General Medical Sciences, Awarded to Herbert Sauro and H. Steven Wiley under Grant U01 CA227544. The associate editor coordinating the review of this article and approving it for publication was G. Jun.

The author is with the Department of Bioengineering, University of Washington, Seattle, WA 98195 USA (e-mail: steveand@uw.edu).

Digital Object Identifier 10.1109/TMBMC.2024.3388977

At a fundamental level, diffusion of molecules that are being investigated, here called probe molecules, arises from thermal motions in the surrounding fluid. Their diffusion coefficients are likewise affected by surrounding molecules, which influence the viscosity of the medium, can act as macromolecular crowders that occupy volume and obstruct diffusive trajectories, and/or can bind to the probe molecules which then slows their movement [1].

These physical behaviors can be treated either explicitly or implicitly in simulations [9]. In the former case, the surrounding molecules are included in the simulation and their effects on diffusion emerge naturally from the simulation results (e.g., [10], [11]); this is a good way to study these effects but is very computationally intensive. In the alternative implicit approach, the surrounding molecules are not included in the simulation directly. Instead, their effects on the probe molecules are accounted for by specifying the appropriate diffusion coefficients in each spatial region (e.g., [8], [12], [13]). This approach is more computationally efficient and adequate in many cases but it requires modeling methods that can be counterintuitive, and which are the focus of this work.

More specifically, this article focuses on how to model interfaces between regions where diffusion coefficients differ. The interfaces can represent membranes that separate well-defined cellular compartments, of which cell and organelle membranes are examples. They can also represent the interfaces between compartments that are not separated by membranes, where examples include the edges of lipid rafts, cytoplasmic droplets, and bacterial nucleoids.

This work represents one of many algorithms that have been developed for the Smoldyn biochemical simulator [14], [15], [16], [17], [18], a particle-based modeling tool that has found substantial use primarily in the biophysics and computational biology research communities (e.g., [19], [20], [21]). Smoldyn is also finding increasing use in the emerging field of molecular communications engineering [22], [23], where the focus is on information transfer via diffusing particles in engineered systems [24], [25], [26], [27]. Recent investigations in each of these fields have highlighted the importance of spatially varying diffusion coefficients in their respective systems (e.g., [28], [29], [30]).

II. System Definition

Figure 1 illustrates the system that we focus on, which has slow diffusion on the left side and fast diffusion on the right. In this case, the difference arises from macromolecular crowders

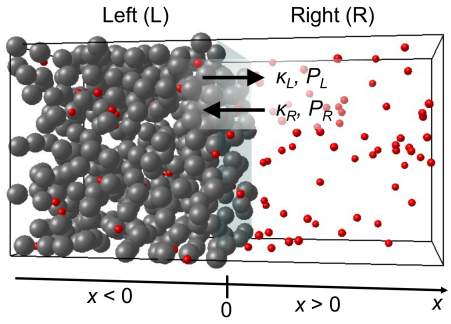

Fig. 1. Illustration of the system considered here, with crowders on the left and none on the right. Probe molecules, shown in red, cross the interface from the left side with transmission coefficient κ_L and transmission probability P_L, and from the right side with κ_R and P_R.

on the left; they don't affect diffusion in the interstitial spaces, where the probe molecules have the same diffusion coefficient on both sides, but instead create a lower effective diffusion coefficient, meaning the diffusion coefficient when measured over a long enough timescale that probe molecules are likely to collide with crowders multiple times, because they obstruct many potential diffusive trajectories [11], [31]. This work is equally focused on systems that have different viscosities on the left and right sides, which are shown to be equivalent below and thus exhibit the same behaviors, but are harder to model explicitly.

The two sides of the system are separated by an interface at $x = 0$ that probe molecules, shown in red, are able to cross. Their transmission through this interface is characterized by the transmission coefficients κ_L and κ_R; κ_L represents transmission *from* the left and κ_R represents transmission *from* the right. These coefficients, which conceptually represent the interface porosity, have units of length/time and range from 0 for a reflecting boundary to ∞ for a perfectly transmitting boundary. As examples, transmission coefficients for lipid bilayers include 3.5×10^8 μm/s for potassium ions, 150 μm/s for water molecules, and 0.014 μm/s for urea molecules [32]. No additional details about the interfaces, including their composition, thickness, or thermodynamics, affect the modeling problem considered here.

For particle-based simulators, we assume the use of the algorithms described in [14], [15], [16], which are implemented in the Smoldyn software. In brief, the simulation uses finite timesteps (Δt), molecules diffuse over each time step with Gaussian-distributed displacements (rms step length is $s = \sqrt{2D\Delta t}$ where D is the diffusion coefficient), and interfaces are infinitessimally thin. When a molecule's trajectory crosses an interface, the molecule is transmitted with probability P_L if it comes from the left and P_R if it comes from the right, and is otherwise reflected.

This work extends these algorithms to allow a molecule's diffusion coefficient to change upon transmission through the interface. In doing so, I found that it was important that the trajectory lengths of transmitted molecules are rescaled so that the diffusion coefficient changes exactly at the interface rather than at the start of the next simulation time step. To do so, the trajectory length that is beyond the interface is multiplied

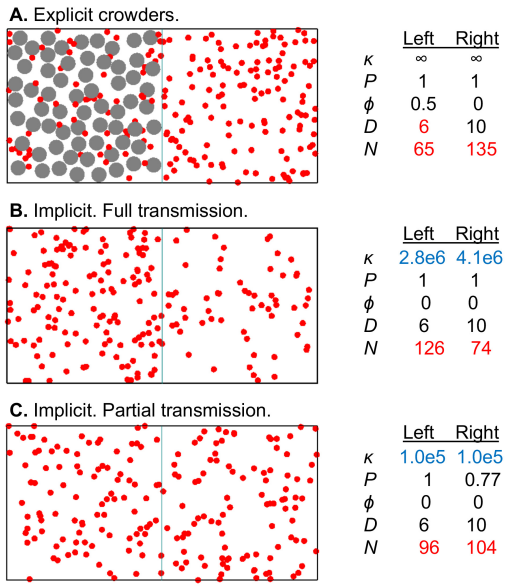

	Left	Right
κ	∞	∞
P	1	1
ϕ	0.5	0
D	6	10
N	65	135

	Left	Right
κ	2.8e6	4.1e6
P	1	1
ϕ	0	0
D	6	10
N	126	74

	Left	Right
κ	1.0e5	1.0e5
P	1	0.77
ϕ	0	0
D	6	10
N	96	104

Fig. 2. Steady-state molecule distribution with 2-dimensional systems. Crowders are shown in gray and probe molecules in red. (A) Crowders were represented explicitly and the interface was fully transmitting in both directions; the probe concentration was lower on the left. (B) Crowders were implicit and the interface was fully transmitting in both directions; the probe concentration was higher on the left. (C) Crowders were implicit and the interface had equal transmission coefficients in the two directions and unequal probabilities; the probe concentration was equal on the two sides. Tables show values for the transmission coefficients (κ, in μm/s), transmission probabilities (P), explicit crowder area occupancies (ϕ), effective diffusion coefficients (D, in μm^2/s), and steady-state numbers of probe molecules on each side (N). Values in black were simulation input parameters and values in red are simulation results. Numerical κ values were computed by inverting (13). See Methods for details.

by the square root of the ratio of the new and old diffusion coefficients.

For a system that has the same diffusion coefficient on each side, [15] shows that the transmission probability ratio equals the transmission coefficient ratio,

$$\frac{P_L}{P_R} = \frac{\kappa_L}{\kappa_R}. \tag{1}$$

That reference also gives exact equations for P_L and P_R [15, eqs. (47)-(48)] as functions of the transmission coefficients, diffusion coefficient, and simulation time step.

III. Results

A. Explicit Simulation With Crowding

Informal observations often suggest that diffusing molecules accrue in regions with slower diffusion coefficients. For example, consider dust on the floor of a room. The dust is produced reasonably evenly throughout the room and yet it builds up near the edges of the floor. The obvious explanation is that the dust has a fast diffusion coefficient in high-traffic regions of the room and a low diffusion coefficient in low-traffic regions, causing it to gradually migrate toward the edges. This supports the notion that lower diffusion coefficients create higher concentrations. This explanation turns out to be correct in some situations, as shown below, but doesn't apply to either the system shown in Figure 1 or to most biochemical systems.

Figure 2(A) shows the actual effect of different diffusion coefficients on molecule concentrations, here with a simulated system that was crowded on the left, empty on the right, and had a fully transmitting interface (see Methods for simulation details). This is a 2 dimensional system to make the image easier to interpret; as shown below, dimensionality doesn't affect quantitative results. The crowders filled $\phi = 50\%$ of the area on the left and were treated explicitly.

I measured effective diffusion coefficients for the two sides by quantifying mean square displacements for probe molecules in nearly identical systems, where their sole differences were that they were either fully crowded or fully uncrowded and they used periodic boundaries to avoid confinement effects. Those simulations showed that the diffusion coefficient on the right side was equal to 10 μm^2/s, in agreement with the value programmed into the simulator, and decreased to 6 μm^2/s on the left due to the crowders.

Simulations of the complete system were run to steady-state, meaning until there was no net flux of molecules across the interface, at which point the probe molecule concentrations were found to be substantially higher on the right side than the left (values are shown as *N* in Figure 2(A)). Thus, the decreased diffusion coefficient on the left does *not* correlate with a higher equilibrium concentration of probe molecules, but with a lower concentration. More precisely, the amount of concentration decrease on the crowded side equaled the volume occupancy by the crowders, implying that the probe molecule concentrations in the accessible areas were the same on both sides.

These results show that crowders have two independent effects. They block diffusive trajectories, which slows effective diffusion coefficients, and they occupy space, which decreases overall equilibrium concentrations. This finding that crowders don't increase concentrations can be understood from thermodynamics: equilibrium concentrations depend only on free energies and not on kinetics, and the crowders don't affect the energies of the probe molecules, so the crowders don't affect their concentrations. The same argument applies to varying viscosities: viscosity does not affect probe molecule energies, so it does not affect their concentrations. Section III-D expands this analysis.

B. Simulators Exhibit Active Diffusion

Figure 2(B) shows a similar simulation, but with the crowders replaced by a slower diffusion coefficient. Molecules diffused with the same diffusion coefficients as above (6 μm^2/s on the left and 10 μm^2/s on the right), the interface was again made fully transmitting in both directions ($P_L = P_R = 1$), and the simulation was also run to steady-state. Its result shows a substantially higher steady-state concentration of probe molecules on the left. This contrasts the explicit simulation result described above, implying that it represents a different physical situation.

To quantify these results analytically, consider a thin layer of thickness l on each side of the interface. The probability that a molecule in the layer on the left of the interface diffuses across the interface during the short time interval Δt is [33]

$$\frac{D_L \Delta t}{l^2}. \tag{2}$$

Multiplying by the concentration on the left side, C_L, yields the molecule flux from left to right. At steady-state, this must equal the flux from right to left, which is derived in the same way, leading to the steady-state equation

$$C_L \frac{D_L \Delta t}{l^2} = C_R \frac{D_R \Delta t}{l^2}. \tag{3}$$

This rearranges to yield the steady-state concentration ratio

$$\frac{C_L}{C_R} = \frac{D_R}{D_L}. \tag{4}$$

This agrees with the simulation result (within stochastic noise).

A physical interpretation of these results is that the different diffusion coefficients represent different amounts of molecule energy, with fast-moving high energy molecules on the right and slow-moving low energy ones on the left (e.g., the right is hot and the left is cold). Over time, molecules tend to settle into lower energy states, so the concentration on the left increases. This is a steady-state result, but it does not represent thermodynamic equilibrium because there is constant energy flow; energy (e.g., in the form of heat) is constantly added to molecules on the right and removed from those on the left. In other words, this simulation represents active diffusion [34], meaning that the diffusing particles are driven by energy that is continuously added to the system, in contrast to the thermal diffusion that is more commonly observed in biochemical systems and discussed elsewhere in this work.

The analogy of dust in a room that was described above is an example of active diffusion, where people walking through the room provide the energy for dust to move from high-traffic areas to low-traffic areas. Chladni plates, which are vibrating surfaces on which sand or other particles accumulate along the surface's nodal lines [35], are another example. Both examples obey the conditions presented in this section, so their steady-state concentrations would presumably be described by (4).

C. Thermal Diffusion Implicit Simulation

To simulate thermal diffusion with implicit methods, one needs to counteract the simulator's tendency to exhibit active diffusion. To do so, we define a virtual membrane at the interface between the two regions and set the transmission coefficients as needed to create the theoretically correct thermal diffusion equilibrium concentration ratio. This ratio is C_L° / C_R°, where degree symbols indicate equilibrium. It equals 1 if probe molecule energies are the same on both sides, which is typical for varying viscosities or non-reactive crowders, and is derived more generally in Section III-D.

The transmission coefficients are defined through the boundary condition equation for the interface [15, eq. (5)]

$$\begin{aligned} D_L \frac{\partial C(x,t)}{\partial x}\bigg|_{x=-0} &= D_R \frac{\partial C(x,t)}{\partial x}\bigg|_{x=+0} \\ &= \kappa_R C(+0,t) - \kappa_L C(-0,t). \end{aligned} \tag{5}$$

Here, each expression represents the net flux toward the left. The first two expressions represent the net flux at the interface

using Fick's law and are equal due to conservation of mass. The third expression represents the difference between the total fluxes from the right and left, respectively. Here and below, the concentration is only considered as a function of one spatial dimension, x, because the interface doesn't affect the concentration in other dimensions.

At equilibrium, the concentration gradients on the two sides are zero, as is the net flux, allowing the simplification

$$\kappa_R C_R^\circ = \kappa_L C_L^\circ, \tag{6}$$

which rearranges to

$$\frac{\kappa_R}{\kappa_L} = \frac{C_L^\circ}{C_R^\circ}. \tag{7}$$

This shows, for example, that equal equilibrium concentrations can be produced by using equal transmission coefficients.

For particle-based simulation, these transmission coefficients need to be converted to transmission probabilities. Following the procedure described in [15], we consider a system that starts at equilibrium with concentrations C_L° and C_R°, and then the simulator diffuses molecules over one time step. It diffuses molecules according to the diffusion coefficient for the region where the molecules begin, and it ignores the presence of the interface initially. After diffusing molecules, but before considering the membrane, the concentration as a function of position is equal to (see [15, eq. (43)])

$$C^{(1)}(x,\Delta t) = \frac{C_L^\circ}{2}\operatorname{erfc}\left[\frac{x}{2\sqrt{D_L\Delta t}}\right] + \frac{C_R^\circ}{2}\operatorname{erfc}\left[\frac{-x}{2\sqrt{D_R\Delta t}}\right]. \tag{8}$$

The first term represents molecules that diffuse from the left and the second represents molecules that diffuse from the right. Next, the simulator transmits molecules that diffused across the interface with probability P_L and P_R, depending on which side the molecule came from. The number of molecules that the simulator transmits from the left to the right is the integral of the first term of (8) from 0 to ∞ times P_L. This result, and the analogous one for transmission the other way, is (see [15, eqs. (44)-(45)])

$$\text{amount from left} = P_L C_L^\circ \sqrt{\frac{D_L\Delta t}{\pi}} \tag{9}$$

$$\text{amount from right} = P_R C_R^\circ \sqrt{\frac{D_R\Delta t}{\pi}}. \tag{10}$$

These need to be equal at equilibrium. Combining them with (7) yields the probability ratio

$$\frac{P_L}{P_R} = \frac{\kappa_L}{\kappa_R}\sqrt{\frac{D_R}{D_L}}. \tag{11}$$

This is one of the central results of this work, extending (1) to account for different diffusion coefficients.

If there is no actual membrane, then $\kappa_L = \kappa_R$ (and are both as large as possible; see below), P_L is equal to 1, and (11) simplifies to

$$P_R = \sqrt{\frac{D_L}{D_R}}. \tag{12}$$

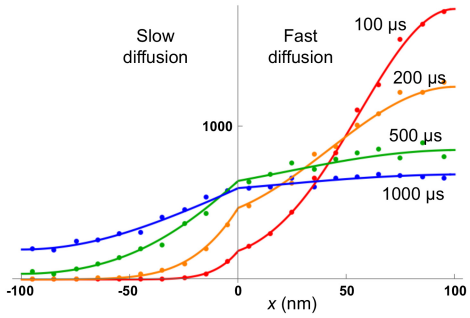

Fig. 3. Comparison of simulation (dots) with numerically integrated results (lines). In this simulation, 10,000 non-interacting molecules started at the far right edge of a 2-dimensional system like that shown in Figure 2(C), and were allowed to diffuse. The diffusion coefficient was 10 μm^2/s for $x \geq 0$ and 3 μm^2/s for $x < 0$, and the interface was maximally transmitting in both directions. Transmission probabilities were $P_L = 1$ and $P_R = 0.55$, from (12). Transmission coefficients were $\kappa_L = \kappa_R = 3.7 \cdot 10^4$ μm/s, found by inverting (13). The y-axis shows numbers of molecules in each 10 nm wide histogram bin at the four time points shown. Numerically integrated results were computed using Mathematica and the boundary conditions from (5).

This probability was used to generate the simulation results shown in Figure 2(C), where it is seen that this probability leads to the correct thermal diffusion result (within stochastic noise) that both sides of the system have the same probe molecule concentrations at equilibrium. This figure was generated with the same diffusion coefficients as before.

These probabilities are also correct away from equilibrium with the result that this algorithm is exact, meaning that its results are statistically identical to those for the underlying continuous-time model system. Figure 3 illustrates this by showing good agreement between simulated and exact concentration profiles for a collection of molecules that all started at the right end of the system at several time points. This system again had fast diffusion on the right and slow diffusion on the left, although with a larger difference to create a more stringent test (3 μm^2/s on the left and 10 μm^2/s on the right).

If there is a membrane, then κ_L and κ_R have smaller values and may differ from each other. In this case, P_L is shown in the appendix to be

$$P_L = \frac{\kappa_L\sqrt{\pi\Delta t}}{c^2\sqrt{D_L}}\left(-1 + \frac{2c}{\sqrt{\pi}} + e^{c^2}\operatorname{erfc}\, c\right), \tag{13}$$

where

$$c = \sqrt{\Delta t}\left(\frac{\kappa_R}{\sqrt{D_R}} + \frac{\kappa_L}{\sqrt{D_L}}\right),$$

and P_R is found from (11).

These equations typically return probabilities that are less than 1, although they can also return larger values if the transmission coefficients are substantially different from each other and time steps are large. This reflects the fact that the simulation method is not quantitatively accurate in this regime due to the transmission rate being slower than it should be, even if the transmission probability is equal to 1 [15]. As an example of an error, suppose $\kappa_L = 0$, $\kappa_R = \infty$, and a molecule starts just barely on the right side of the interface. Ideally, the molecule would be essentially certain to cross the barrier over any finite amount of time, but in any single time step, the simulated crossing probability would only be up to

50% due to the possibility of the molecule diffusing in the opposite direction. The best solution to this problem is to cap the larger probability value to 1 and to use (12) for the other value. This produces the correct concentration ratio but lower transmission rates than desired.

Inverting (11) and (13), of which the latter has to be done numerically, yields κ_L and κ_R from P_L and P_R. If one of the probability values is equal to 1, then this approach returns the maximum simulated transmission coefficient that is possible with the given time step. These values are listed in Fig. 2 and the Fig. 3 caption.

D. Concentration Ratio Derivation

Here, we solve for the equilibrium concentration ratio, which is required in (7). From thermodynamics, it depends on entropic and enthalpic contributions (the enthalpy is essentially identical to the energy for most biochemical contexts).

The entropic component simply reflects the accessible volume on the two sides of the system. In particular, for crowders that occupy volume fraction ϕ, the accesible volume in some region relates to the total volume of that region, V, as

$$V_{acc.} = (1-\phi)\,V. \tag{14}$$

Based on this, the ratio of the probabilities of a molecule being on the left and right side of the system is

$$\frac{p_L}{p_R} = \frac{V_L(1-\phi_L)}{V_R(1-\phi_R)}, \tag{15}$$

where V_L and V_R are the volumes of the two sides.

The enthalpic contribution reflects the interactions of a molecule with crowders or other components on the two system sides. If the probe molecules only interact with crowders by colliding with them, then this doesn't affect their enthalpies, and we can set $H_L = H_R = 0$. On the other hand, probe molecules that do bind to the crowders have decreased enthalpies. Likewise, probe molecule interactions with other surrounding molecules, such as solvated ions, can also affect enthalpies. For generality, we assume probe molecules have enthalpies of H_L and H_R on the given sides; Section III-E derives these values for incomplete binding to crowders.

The Boltzmann distribution states that the probability of a molecule being in some state is proportional to $e^{-H/k_B T}$, where H is the enthalpy of the state, k_B is Boltzmann's constant, and T is the absolute temperature (which must be uniform throughout the system for equilibrium thermodynamics to apply). In this case, the two states are the two sides of the system. Thus, the enthalpic contributions lead to the probability ratio

$$\frac{p_L}{p_R} = \frac{e^{-H_L/k_B T}}{e^{-H_R/k_B T}} = e^{-\Delta H/k_B T}, \tag{16}$$

where $\Delta H = H_L - H_R$.

Multiplying the entropic and enthalpic probability contributions, and also dividing probabilities by volumes, yields the equilibrium concentration ratio

$$\frac{C_L^\circ}{C_R^\circ} = \frac{1-\phi_L}{1-\phi_R}\, e^{-\Delta H/k_B T}. \tag{17}$$

For noninteracting probe molecules, this ratio is 1 for uncrowded systems (Figure 2(C)) and represents the crowding fraction for crowded systems (Figure 2(A)). Note that (17) is independent of the diffusion coefficients, showing again that differences in thermal diffusion coefficients do not affect equilibrium concentrations. Also note that (17) is independent of system dimensionality, thus validating the mixed use of 1D, 2D, and 3D within this work.

E. Enthalpies for Incomplete Crowder Binding

Unfortunately, (17) is rarely practical on its own because only some fraction of the probe molecules are typically bound to crowders at any given time. Thus, one needs to average the binding enthalpy over all probe molecules, including both the bound and unbound ones.

To account for this equilibrium condition, we start by assuming the chemical reaction

$$\mathrm{X} + \mathrm{S} \underset{k_d}{\overset{k_a}{\rightleftharpoons}} \mathrm{XS}, \tag{18}$$

where X is a probe molecule, S is a binding site on a crowder molecule, and k_a and k_d are the association and dissociation rate constants. This reaction has dissociation constant $K_d = k_d/k_a$, from which the binding enthalpy is

$$H_b = H_b^{\mathrm{std}} + k_B T \ln \frac{K_d}{C^{\mathrm{std}}}, \tag{19}$$

where C^{std} is a standard concentration and H_b^{std} is the binding enthalpy when the dissociation constant is equal to that standard concentration.

If the scaled dissociation constant, K_d/C^{std}, is much less than 1, representing tight binding, then this H_b is the H_L value from above (for crowders on the left) and the problem is solved. Vice versa, if the scaled dissociation constant is much more than 1, representing very weak binding, then this H_b is irrelevant because the probe molecules aren't spending a significant amount of time bound to crowders anyhow; in that case, H_L can be set to zero and binding is ignored. For cases in between these limits, we need to consider both the bound and unbound states, which we solve next.

Once a molecule binds to a crowder, it spends a mean time $\tau_b = 1/k_d$ bound to that crowder before releasing. Then, it spends a mean time $\tau_u = 1/(k_a[\mathrm{S}])$ in its unbound state before rebinding to another crowder, where [S] is the crowder binding site concentration. Combining these, substituting with the dissociation constant, and simplifying gives the fraction of time that a molecule is bound to a crowder as

$$f_b = \frac{\tau_b}{\tau_b + \tau_u} = \frac{[\mathrm{S}]}{K_d + [\mathrm{S}]}. \tag{20}$$

The bound and unbound states are mutually exclusive, so the probability factor for a molecule being on the left side of the system, $\exp(-H_L/k_B T)$, is equal to the sum of the probability factors for the bound and unbound states,

$$e^{-H_L/k_B T} = f_b\, e^{-H_b/k_B T} + (1-f_b)\, e^{0/k_B T}. \tag{21}$$

The exponent in the latter term represents the fact that the enthalpy of the unbound state is taken as zero. Rearranging gives the left side energy term as

$$H_L = k_B\,T \ln \frac{K_d + [\mathrm{S}]}{K_d + [\mathrm{S}] \exp\left(-H_b^{\mathrm{std}}/k_B\,T\right) C^{\mathrm{std}}/K_d}. \quad (22)$$

It's straightforward to check that this result has the correct behavior in the limits of tight and weak binding, yielding (19) and $H_L \approx 0$, respectively.

IV. Conclusion

This article addresses the question of how to efficiently simulate molecular diffusion between regions that have different diffusion coefficients. It shows that there is a distinction between active diffusion, in which molecule motion is driven by energy that is continuously added to the system, and thermal diffusion, which occurs even at thermodynamic equilibrium. This difference affects whether molecules accumulate in regions with slow diffusion. Actively diffusing molecules do accumulate because slower diffusion corresponds to lower energies, while thermally diffusing molecules do not accumulate because slower diffusion typically arises from macromolecular crowding or higher viscosity, which do not affect molecule energies.

Active diffusion can arise in both biochemical [34], [36] and molecular communication [26] systems. In its case, (4) shows that steady-state concentrations scale inversely with diffusion coefficients. These results appear naturally in particle-based simulations (Figure 2(B)).

On the other hand, biochemical and molecular communication systems are typically too small to have internal thermal gradients, and do not drive molecules externally, so their molecules diffuse thermally. In these cases, explicit simulation (Figure 2(A)) of diffusion coefficient changes is accurate but computationally expensive. This makes implicit simulation (Figure 2(C)) generally preferable, but one needs to counteract the simulators' tendency to exhibit active diffusion. This can be achieved as follows. (1) Compute the equilibrium concentration ratio for the two regions; it is equal to 1 if volume exclusion and binding enthalpy are negligible and given by (17) for the general case. If there is weak binding between the probe molecules and crowders, the enthalpy for this equation is given by (22). (2) Compute the transmission coefficient ratio from (7). (3) Compute the transmission probabilities from (11) and either (12) for an interface without a membrane or (13) for an interface with a membrane.

These new algorithms have been implemented in the Smoldyn software. They are also accessible through the `surfacetransmit` function in the public domain code library SurfaceParam.c (included in the Smoldyn download package). This function computes P_L and P_R from κ_L and κ_R using (12) and (13). It can also invert this calculation to return κ_L and κ_R from P_L and P_R, which it performs using a greedy random walk algorithm.

V. Methods

All simulations were run in Smoldyn 2.72 [16], [17]. Most of the results shown in Figure 2 used the following simulation parameters: crowders had a 5 nm radius and 1 μm^2/s diffusion coefficient; probe molecules were point-like to prevent interactions between probes, had a 10 μm^2/s diffusion coefficient in most cases, and a 6 μm^2/s diffusion coefficient on the left side of panels B and C; the system was 200 nm long by 100 nm high with reflective boundaries and had a membrane in the middle of the system; simulations investigated 11 ms of time in 0.01 μs time steps; and there were 200 probe molecules initially distributed evenly throughout the system. All simulations were equilibrated for 1 ms before data collection and then data were collected over the subsequent 10 ms. Simulations to confirm the probe molecule diffusion coefficient on the right side of Figure 2(A), and to measure the effective diffusion coefficient on the left side of the same figure, were essentially the same; however, their systems were reduced to only the appropriate side of the full system and were given periodic boundaries in order to remove confinement effects.

All simulation files obey MIRIAM guidelines [37] and are available at the archive https://www.smoldyn.org/archive.

Appendix

Eqs. (9) and (10) describe how much concentration actually crosses the interface during one simulation time step, using transmission probabilities P_L and P_R. Equating this with how much concentration should cross the interface during the same amount of time, using transmission coefficients κ_L and κ_R, creates equations that relate these sets of parameters. We follow the procedure described in [15, Appendix B] to solve the problem: suppose the concentration is 0 for $x < 0$ and is C_R for $x > 0$ at time 0; how much substance is in the $x < 0$ region of the system at time t?

The one-dimensional diffusion equation is

$$\frac{\partial C(x,t)}{\partial t} = D(x)\frac{\partial^2 C(x,t)}{\partial x^2}. \quad (23)$$

Laplace transforming this, using $C_L(x,t)$ for the concentration on the left, $C_R(x,t)$ for the concentration on the right, and hats for their Laplace transformed versions, yields

$$-C_L(x,0) + z\hat{C}_L(x,z) = D_L\frac{\partial^2 \hat{C}_L(x,z)}{\partial x^2} \quad (24)$$

$$-C_R(x,0) + z\hat{C}_R(x,z) = D_R\frac{\partial^2 \hat{C}_R(x,z)}{\partial x^2}. \quad (25)$$

Boundary conditions for these equations include:

$$C_L(x,0) = 0 \quad (26)$$

$$C_R(x,0) = C_R \quad (27)$$

$$\hat{C}_L(-\infty,z) = 0 \quad (28)$$

$$\hat{C}_R(\infty,z) = \frac{C_R}{z}. \quad (29)$$

Simplifying (24) and (25) with these boundary conditions and solving yields the general solutions with unknown constants a and b,

$$\hat{C}_L(x,z) = ae^{x\sqrt{\frac{z}{D_L}}} \quad (30)$$

$$\hat{C}_R(x,z) = \frac{C_R}{z} + be^{-x\sqrt{\frac{z}{D_R}}}. \tag{31}$$

Additional boundary conditions arise from the conservation of flux over the interface, given by the Laplace transformed version of (5),

$$D_L \frac{\partial \hat{C}_L(x,z)}{\partial x}\bigg|_{x=-0} = D_R \frac{\partial \hat{C}_R(x,z)}{\partial x}\bigg|_{x=+0} \tag{32}$$

$$= \kappa_R \hat{C}_R(+0,z) - \kappa_L \hat{C}_L(-0,z). \tag{33}$$

These boundary conditions allow solution of a and b, yielding

$$a\sqrt{D_L} = -b\sqrt{D_R} = \frac{C_R\kappa_r}{z\left(\sqrt{z} + \kappa_R D_R^{-1/2} + \kappa_L D_L^{-1/2}\right)}. \tag{34}$$

This is substituted into (30) and the result is integrated from $-\infty$ to 0 to yield

$$\hat{M}(z) = \int_{-\infty}^{0} \hat{C}_L(x,z)\,dx = \frac{C_R\kappa_r z^{-3/2}}{\sqrt{z} + \kappa_R D_R^{-1/2} + \kappa_L D_L^{-1/2}}. \tag{35}$$

This inverse Laplace transforms to yield the desired solution

$$M(t) = \frac{C_R\kappa_R t}{c^2}\left(-1 + \frac{2c}{\sqrt{\pi}} + e^{c^2}\operatorname{erfc} c\right), \tag{36}$$

where

$$c = \sqrt{t}\left(\frac{\kappa_R}{\sqrt{D_R}} + \frac{\kappa_L}{\sqrt{D_L}}\right) = \sqrt{2}\left(\kappa'_L + \kappa'_R\right). \tag{37}$$

This final expression uses reduced units, in which

$$\kappa'_L = \frac{\kappa_L\sqrt{t}}{\sqrt{2D_L}} \kappa'_R = \frac{\kappa_R\sqrt{t}}{\sqrt{2D_R}}. \tag{38}$$

This solution can be used to find the transmission probability for a particle-based simulator. Eq. (10) gives the amount of substance that is actually transmitted in a simulation and (36) gives the amount that should be transmitted. Equating these two expressions and solving for the transmission probability yields

$$P_R = \frac{\kappa'_R\sqrt{2\pi}}{c^2}\left(-1 + \frac{2c}{\sqrt{\pi}} + e^{c^2}\operatorname{erfc} c\right). \tag{39}$$

The corresponding P_L equation is presented as (13).

ACKNOWLEDGMENT

The author thanks Grant Bowman for inspiring this work and Herbert Sauro and H. Steven Wiley for useful discussions.

REFERENCES

[1] J. A. Dix and A. Verkman, "Crowding effects on diffusion in solutions and cells," *Annu. Rev. Biophys.*, vol. 37, pp. 247–263, Jun. 2008.
[2] M. B. Elowitz, M. G. Surette, P.-E. Wolf, J. B. Stock, and S. Leibler, "Protein mobility in the cytoplasm of escherichia coli," *J. Bacteriol.*, vol. 181, no. 1, pp. 197–203, 1999.
[3] S. Stylianidou, N. J. Kuwada, and P. A. Wiggins, "Cytoplasmic dynamics reveals two modes of nucleoid-dependent mobility," *Biophys. J.*, vol. 107, no. 11, pp. 2684–2692, 2014.
[4] C. P. Brangwynne et al., "Germline P granules are liquid droplets that localize by controlled dissolution/condensation," *Science*, vol. 324, no. 5935, pp. 1729–1732, 2009.
[5] P. Li et al., "Phase transitions in the assembly of multivalent signalling proteins," *Nature*, vol. 483, no. 7389, pp. 336–340, 2012.
[6] C. Dietrich, B. Yang, T. Fujiwara, A. Kusumi, and K. Jacobson, "Relationship of lipid rafts to transient confinement zones detected by single particle tracking," *Biophys. J.*, vol. 82, no. 1, pp. 274–284, 2002.
[7] E. Zavala and T. T. Marquez-Lago, "The long and viscous road: Uncovering nuclear diffusion barriers in closed mitosis," *PLoS Comput. Biol.*, vol. 10, no. 7, 2014, Art. no. e1003725.
[8] S. M. Mustam, S. K. Syed-Yusof, and S. Zubair, "Capacity and delay spread in multilayer diffusion-based molecular communication (DBMC) channel," *IEEE Trans. Nanobiosci.*, vol. 15, no. 7, pp. 599–612, Oct. 2016.
[9] S. Smith and R. Grima, "Fast simulation of Brownian dynamics in a crowded environment," *J. Chem. Phys.*, vol. 146, no. 2, 2017, Art. no. 24105.
[10] S. R. McGuffee and A. H. Elcock, "Diffusion, crowding & protein stability in a dynamic molecular model of the bacterial cytoplasm," *PLoS Comput. Biol.*, vol. 6, no. 3, 2010, Art. no. e1000694.
[11] S. S. Andrews, "Effects of surfaces and macromolecular crowding on bimolecular reaction rates," *Phys. Biol.*, vol. 17, no. 4, 2020, Art. no. 45001.
[12] S. M. Mustam, S. K. S. Yusof, and S. Nejatian, "Multilayer diffusion-based molecular communication," *Trans. Emerg. Telecommun. Technol.*, vol. 28, no. 1, 2017, Art. no. e2935.
[13] M. M. Al-Zubi and A. S. Mohan, "Modelling of multilayer biological medium under molecular communication paradigm," in *Proc. IEEE Life Sci. Conf. (LSC)*, 2017, pp. 31–34.
[14] S. S. Andrews and D. Bray, "Stochastic simulation of chemical reactions with spatial resolution and single molecule detail," *Phys. Biol.*, vol. 1, no. 3, p. 137, 2004.
[15] S. S. Andrews, "Accurate particle-based simulation of adsorption, desorption and partial transmission," *Phys. Biol.*, vol. 6, no. 4, 2009, Art. no. 46015.
[16] S. S. Andrews, N. J. Addy, R. Brent, and A. P. Arkin, "Detailed simulations of cell biology with Smoldyn 2.1," *PLoS Comput. Biol.*, vol. 6, no. 3, 2010, Art. no. e1000705.
[17] S. S. Andrews, "Smoldyn: Particle-based simulation with rule-based modeling, improved molecular interaction and a library interface," *Bioinformatics*, vol. 33, no. 5, pp. 710–717, 2017.
[18] S. S. Andrews, "Rule-based modeling using wildcards in the Smoldyn simulator," in *Modeling Biomolecular Site Dynamics* (Methods in Molecular Biology). New York, NY, USA: Humana Press, 2019, pp. 179–202.
[19] V. V. Matveev, "Close agreement between deterministic versus stochastic modeling of first-passage time to vesicle fusion," *Biophys. J.*, vol. 121, no. 23, pp. 4569–4584, 2022.
[20] R. Taylor, J. Allard, and E. L. Read, "Simulation of receptor triggering by kinetic segregation shows role of oligomers and close contacts," *Biophys. J.*, vol. 121, no. 9, pp. 1660–1674, 2022.
[21] K. Guan, E. R. Curtis, D. J. Lew, and T. C. Elston, "Particle-based simulations reveal two positive feedback loops allow relocation and stabilization of the polarity site during yeast mating," *PLoS Comput. Biol.*, vol. 19, no. 10, 2023, Art. no. e1011523.
[22] A. Abdali and M. Kuscu, "Frequency-domain model of microfluidic molecular communication channels with graphene bioFET-based receivers," 2023, *arXiv:2307.04229*.
[23] M. Civas, M. Kuscu, and O. B. Akan, "Frequency-domain detection for molecular communication with cross-reactive receptors," 2023, *arXiv:2309.09377*.
[24] M. Pierobon and I. F. Akyildiz, "Diffusion-based noise analysis for molecular communication in nanonetworks," *IEEE Trans. signal Process.*, vol. 59, no. 6, pp. 2532–2547, Jun. 2011.
[25] H. B. Yilmaz, A. C. Heren, T. Tugcu, and C.-B. Chae, "Three-dimensional channel characteristics for molecular communications with an absorbing receiver," *IEEE Commun. Lett.*, vol. 18, no. 6, pp. 929–932, Jun. 2014.
[26] N. Farsad, H. B. Yilmaz, A. Eckford, C.-B. Chae, and W. Guo, "A comprehensive survey of recent advancements in molecular communication," *IEEE Commun. Surveys Tuts.*, vol. 18, no. 3, pp. 1887–1919, 3rd Quart., 2016.
[27] F. Zabini, "Spatially distributed molecular communications: An asynchronous stochastic model," *IEEE Commun. Lett.*, vol. 22, no. 7, pp. 1326–1329, Jul. 2018.
[28] D. P. Trinh, Y. Jeong, C.-B. Chae, and S.-H. Kim, "Molecular communication in inhomogeneous diffusion channels," *IEEE Wireless Commun. Lett.*, vol. 11, no. 9, pp. 1975–1979, Sep. 2022.

[29] L. Mantovanelli, D. S. Linnik, M. Punter, H. J. Kojakhmetov, W. M. Śmigiel, and B. Poolman, "Simulation-based reconstructed diffusion unveils the effect of aging on protein diffusion in escherichia coli," *PLoS Comput. Biol.*, vol. 19, no. 9, 2023, Art. no. e1011093.

[30] Y. M. Ahmed and G. R. Bowman, "Phospho-signaling couples polar asymmetry and proteolysis within a membraneless microdomain in C. crescentus," bioRxiv, 2023, Preprint.

[31] I. L. Novak, P. Kraikivski, and B. M. Slepchenko, "Diffusion in cytoplasm: Effects of excluded volume due to internal membranes and cytoskeletal structures," *Biophys. J.*, vol. 97, no. 3, pp. 758–767, 2009.

[32] S. Paula, A. Volkov, A. Van Hoek, T. Haines, and D. W. Deamer, "Permeation of protons, potassium ions, and small polar molecules through phospholipid bilayers as a function of membrane thickness," *Biophys. J.*, vol. 70, no. 1, pp. 339–348, 1996.

[33] C. Gardiner, K. McNeil, D. Walls, and I. Matheson, "Correlations in stochastic theories of chemical reactions," *J. Stat. Phys.*, vol. 14, pp. 307–331, Apr. 1976.

[34] C. P. Brangwynne, G. H. Koenderink, F. C. MacKintosh, and D. A. Weitz, "Intracellular transport by active diffusion," *Trends Cell Biol.*, vol. 19, no. 9, pp. 423–427, 2009.

[35] I. Grabec and N. Sok, "Diffusion equation generalized for modeling of Chladni patterns," *Strojniški Vestnik J. Mech. Eng.*, vol. 69, nos. 5–6, pp. 284–286, 2023.

[36] N. Van Kampen, "Diffusion in inhomogeneous media," *J. Phys. Chem. Solids*, vol. 49, no. 6, pp. 673–677, 1988.

[37] N. Le Novère et al., "Minimum information requested in the annotation of biochemical models (MIRIAM)," *Nat. Biotechnol.*, vol. 23, no. 12, pp. 1509–1515, 2005.